Available online at www.sciencedirect.com
ScienceDirect
Journal of the European Ceramic Society 28 (2008) 1129–1134
www.elsevier.com/locate/jeurceramsoc

Solute and defect segregation at the space charge layers of Fe-doped fine-grained Al_2O_3: Effect on the creep rate

A. Bataille [a,*], A. Addad [a], C. Courtois [b], T. Duhoo [a], J. Crampon [a]

[a] *Laboratoire de Structure et Propriétés de l'Etat Solide, UMR-CNRS 8008, Bât. C6 - Cité Scientifique, Université des Sciences et Technologies de Lille, 59 655 VILLENEUVE D'ASCQ, Cedex, France*
[b] *Laboratoire des Matériaux et Procédés, E.A. 4015, Université de Valenciennes et du Hainaut Cambrésis, Z.I. du Champ de l'Abbesse, 59600 MAUBEUGE, France*

Received 24 March 2007; received in revised form 12 September 2007; accepted 30 September 2007

Abstract

Compressive creep in air of vacuum hot-pressed undoped alumina and 0.5 at.% iron doped alumina materials was investigated. The dark green colour of doped alumina accounted for the presence of iron as Fe^{2+} species at first. Also, iron rich precipitates were observed and identified as $FeAl_2O_4$ spinel. During the tests, Fe^{2+} species underwent oxidation during creep. The space charge concept is developed to account for the data and the interaction between the space charge and the extrinsic defect species. The observed iron segregation is proposed in the subgrain boundary region. Iron spinel precipitates were observed interacting with grain boundaries. Oxidation of Fe^{2+} resulted in Fe^{3+}, which segregated into the grain boundaries. This segregation produced creep resistance of alumina.

Keywords: Al_2O_3; Creep; Defects; Grain boundary; Space charge

1. Introduction

When studying the effect of additives on the diffusion creep of polycrystalline alumina, the cation doping can affect the creep behaviour through several microstructural features such as grain size, porosity, and secondary phase formation. Indeed, the diffusion controlling mechanism depends on atomic defect population and concentration but also on the complex nature of the interfaces when different phases are present. Moreover, the creep deformation of Fe-containing alumina is related to the mixed valence of the doping cation and to its possible evolution with the temperature and the testing atmosphere.[1–3] The related solubility of the mixed valence Fe cation can result in precipitation and in the formation of composite interfaces between alumina grains and those precipitates.[4,5] The effects of iron have been observed and discussed in Fe-doped alumina through sintering studies, creep investigations and conductivity monitoring and also through grain growth observations. Results have been mainly collected on alumina materials with grain sizes from 10 up to 200 μm.[1–4,6–9] Drahus *et al.*[10] presented recently a study on the sintering of Fe-doped alumina with micrometric grain sizes.

A previous paper has reported the compressive creep rate behaviour of 1 at.% Fe-doped fine-grained alumina.[5] Effects of precipitation, grain growth and cavitation occurring during creep tests were discussed in this paper. In the present paper, complementary creep tests were carried out at lower Fe-doped alumina (0.5 at.%) and under the same conditions ($\sigma = 75$ MPa, $T = 1400\,^{\circ}C$). The observed compressive creep behaviour of 0.5 at.% Fe-doped fine-grained alumina was similar to that observed and described with the 1 at.% Fe-doped fine-grained alumina.

The incidence of grain growth and cavitation on creep is not the object of the present paper. The presented experimental results are not due to the change of the microstructure and the related discussion hereafter will consider isostructural conditions.

This paper will focus on the role of space charge on the prevalent point defects associated with matter transport in crept Fe-doped alumina. The existence of the space charge potential has been observed experimentally in undoped[11] and Mg,[12–14] Fe,[15–16] Ti and Li[17] doped Al_2O_3. The segregation of aliovalent

* Corresponding author. Tel.: +33 320 434861; fax: +33 320 436591.
E-mail address: Alain.Bataille@univ-lille1.fr (A. Bataille).

0955-2219/$ – see front matter © 2007 Elsevier Ltd. All rights reserved.
doi:10.1016/j.jeurceramsoc.2007.09.054

solutes and defects to the grain boundaries or to the subgrain boundary regions can be substantially modified by the space charge potential. During creep in air of Fe-doped alumina, hot-pressed under reducing conditions, the valence of the Fe content is continuously changing. The nature and the concentration of the point defects controlling the creep strain rate evolve and there is consequently a complex dynamic redistribution of defects and solutes in the grain boundaries and space charge layers of alumina, assuming reduction–oxidation mechanisms of the Fe dopant.

2. Experimental procedure

Overall experimental procedures corresponding to this study were identical to those described in a previous paper.[5] The powder used was a high-purity α-Al_2O_3 (SM8, >99.98% pure, Baikowski, France) with an average grain size of 0.3 μm. 0.5 at.% Fe-doped alumina was obtained by mixing the powder in deionized water, together with the appropriate addition of aliquot of high-purity $Fe(NO_3)_3{\cdot}6H_2O$ solution. After calcination at 800 °C in air for 2 h, the doped powder was hot-pressed under secondary vacuum, in a graphite die, under $\sigma = 45$ MPa at 10 °C/min up to 1450 °C.[5] Undoped alumina powder was also hot pressed in the same reducing conditions.

Scanning electron microscopy (SEM) and analytical transmission electron microscopy (TEM-Philips CM 30, Noran X-ray EDS) were used to observe the microstructure. For SEM observations, the microstructure was revealed by thermal etching in air at $T = 1400$ °C for 90 min. The mean grain sizes were calculated[18] by multiplying the square root of the average grain surface by 1.38. Specimens for compression tests were 7 mm high and had a square cross-section of 3 mm × 3 mm. The load was applied parallel to the hot pressing axis. Compressive creep tests were carried out in air at 1400 °C, under a stress of 75 MPa and up to different true strains.

3. Results

The resulting densities of the undoped and Fe-doped alumina were, respectively, 97.5 and 99.5% of the theoretical one. The microstructure of both materials was homogeneous and equiaxed, and the grain size of the undoped alumina was 1.4 μm whereas it was 1.6 μm for the Fe-doped material.

The observed effect of the Fe doping on creep strain rate under previously described conditions is shown in Fig. 1. The creep true strain rate versus true strain curve presented two distinct sequences: following classical transient, a quasi steady state creep rate was reached during a first stage up to a compressive true strain of about $\varepsilon = -15\%$, then, the true strain rate decreased strongly, and a second quasi steady state creep stage was observed. Creep strain rate changes occurred in the narrow range of true strains [−14, −17%] for all tested samples of Fe-doped alumina. Under the compressive true stress of $\sigma = 75$ MPa, the true strain rate was about $9 \times 10^{-5}\ s^{-1}$ in the first stage, whereas it was about $2 \times 10^{-5}\ s^{-1}$ in the second stage. In the same conditions, the undoped specimen showed only one stage with a quasi steady state strain rate of about $5 \times 10^{-5}\ s^{-1}$.

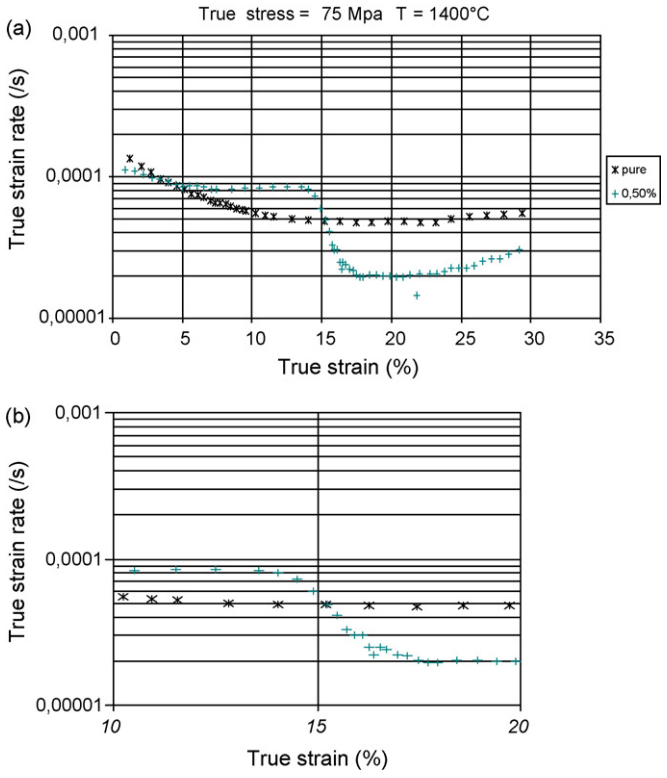

Fig. 1. True strain rate versus true strain curves under $\sigma = 75$ MPa and at $T = 1400$ °C. 0.5 Cat.% Fe-doped alumina (+ symbol) and pure alumina (× symbol). (a) True strain range [0, −30%], (b) true strain range [−10, −20%]. Fe-doped alumina presented two stages for the strain rate when pure alumina deformed at a quasi steady state strain rate.

It has been shown previously[5] that the grain growth of the 1 at.% Fe-doped material was very limited in the strain range $\varepsilon = [-10, -20\%]$, where the decrease of the creep rate occurred. In the present work, the corresponding final grain sizes of the 0.5 at.% Fe-doped and undoped alumina were, respectively, 4.1 and 3.2 μm for the maximum true strain. No abnormal grain growth was observed in the microstructure of deformed specimens. Fe-cation segregation was detected in grain boundary regions, by analytical TEM investigations, in 0.5 at.% Fe-doped alumina specimen crept up to −23% (Fig. 2). In a specimen crept in the early stage of deformation (up to about $\varepsilon = -5\%$), iron rich precipitates were observed and identified as $FeAl_2O_4$ spinel. It shall be noticed that some of these precipitates were observed interacting with grain boundaries (Fig. 3).

The bulk remained dark-green coloured during the first stage and underwent rapid colouration change within the mentioned strain range, i.e. within [−14, −17%]. In this narrow true strain range, the bulk colour was a bright red. Eventually the bulk colour turned to a creamy white.

4. Discussion

In the present work as in our previous study,[5] the grain size (1.4–2.6 μm) of the samples was finer than that of the earlier similar studies (up to 200 μm) published before the 1990's.[1–3,7,19]

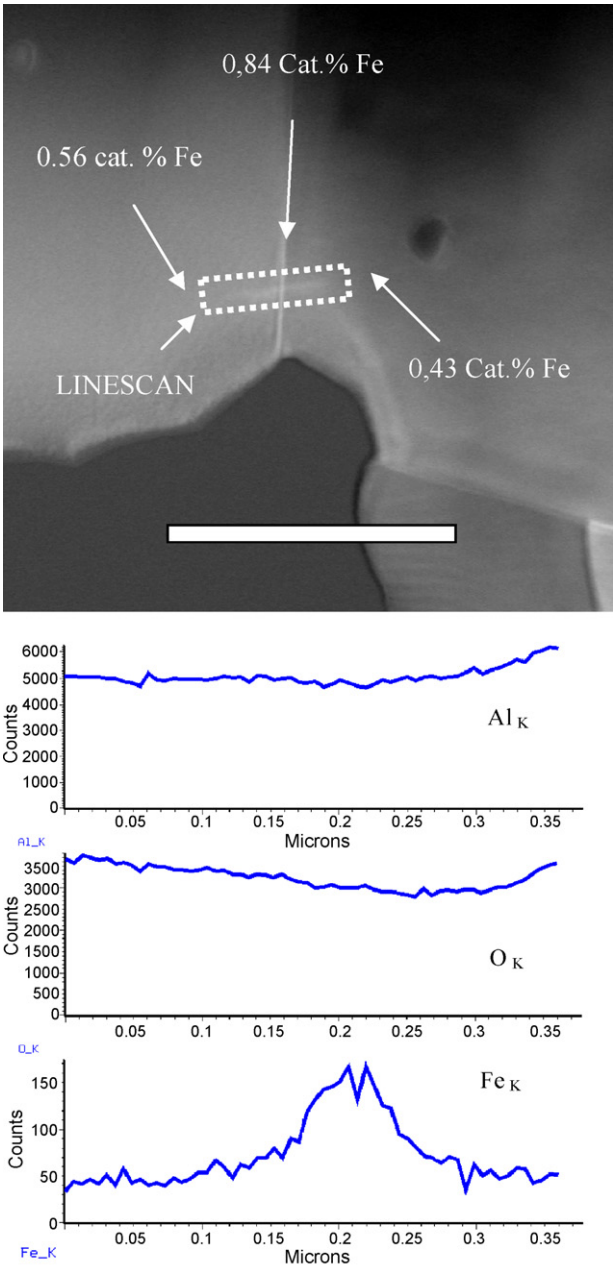

Fig. 2. Grain boundary iron concentration compared to bulk (scale bar: 1 μm, linescan: 0.35 μm). Iron doped sample deformed up to $\varepsilon = -23\%$.

A direct comparison of the creep strain rate data, between undoped and doped alumina, in Fig. 1 is not strictly possible because of the little difference in initial grain sizes. However, these data can be used to assess the effect of Fe doping on the alumina grain boundary diffusivity. In order to rationalize our results, we will hereafter discuss the consequence on the creep behaviour of alumina (i) due to the defect chemistry in terms of space charge formation, (ii) due to the resulting redistribution of defects and solutes in the grain boundaries and subgrain boundary regions, (iii) due to the oxidation of Fe^{2+} and oversized species segregation in the grain boundary.

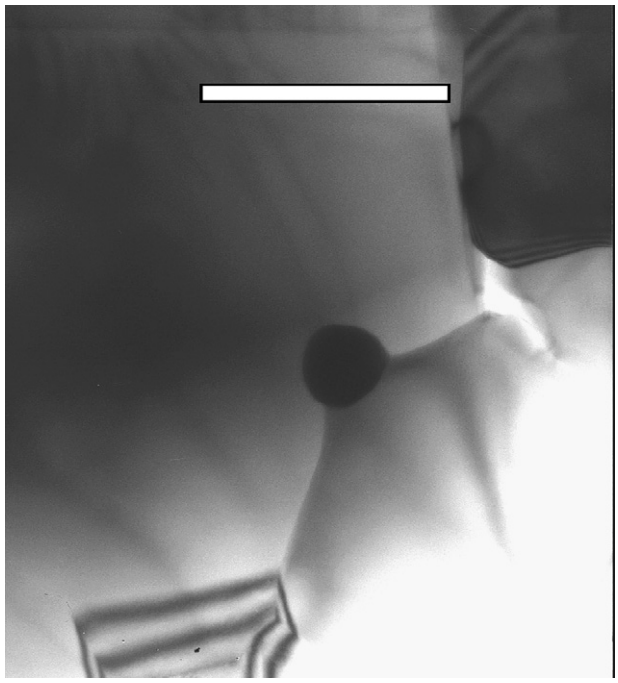

Fig. 3. Observation of a $FeAl_2O_4$ spinel precipitate interacting with a grain boundary (scale bar: 1 μm). Iron doped sample deformed up to $\varepsilon = -5$.

4.1. Defect chemistry and space charge formation

Pure and doped Al_2O_3 are expected to have defect concentrations at the grain boundaries that are different from those in the bulk, with a corresponding difference in electrical potential between the two regions. This unbalance results in a net charge on the grain boundary with a balancing opposite charge in the subgrain boundary region. Either Schottky-type or Frenkel-type disorders may be of importance in pure Al_2O_3.

The sign of the boundary charge in pure alumina is essentially determined by the relative magnitudes of the formation free energies of the individual defects involved in the dominant intrinsic disorder. Related recent results[11] on grain boundary migration in undoped alumina, under an external electric field, have provided experimental evidence that the grain boundaries of Al_2O_3 carry a positive electric charge resulting from the presence of excess Al^{3+} ions. In such a situation, it has been suggested[11] that the fast oxygen diffusivity along the grain boundary, relative to the aluminium one, may be related to the segregation of oxygen vacancies which contribute to the building up of the positively charged grain boundaries. The cation sites on the boundary are occupied primarily by Al^{3+} ions, whereas most of the anion sites on the boundary are empty. For Jeong *et al.*[11] who assume that a cation Frenkel mechanism dominates, this corresponds to a positive grain boundary contiguous to which, in the Kroeger and Vink[20] defect notation, V'''_{Al} are segregated while $Al_i^{\bullet\bullet\bullet}$ and $V_o^{\bullet\bullet}$ are depleted in the compensating space charge subgrain boundary region.

However, even if recent theoretical studies[21–25] concerning the determination of the dominant intrinsic disorder show differences, all calculations of the possible intrinsic defect mechanisms give formation free energies, for the Schottky-type or

Frenkel-type disorders, between 4 and 10 eV/defect.[21–32] Due to these high values, concentrations of intrinsic point defects at high temperature are expected to be quite small in Al_2O_3. Thus, all other experimental measurements showing the existence[12–17] and the positive sign[12–14,17] of the grain boundary charge in alumina have been reported for effectively doped Al_2O_3.

For Al_2O_3 doped with an acceptor such as Fe, both neutral Fe_{Al}^{x} and ionized Fe'_{Al} foreign point defects are involved. The segregation of these defects in the grain boundary or subgrain boundary regions alters defect concentrations at the grain boundary, in the subgrain boundary space charge and in the bulk.[8] It is now well accepted that both the ionic size difference (resulting in elastic misfit strain energy) as well the valence (resulting in charge compensation) contribute to the driving force for segregation. Considering only the ionic charge (i.e. ignoring the difference in ionic radius), when $[Fe'_{Al}]$ is higher than $[Fe_{Al}^{x}]$, the ionized Fe'_{Al} foreign point defects can be considered to be ideal aliovalent solutes. In terms of compensating defect mechanisms, two possibilities of mechanism result in either aluminium interstitials if Frenkel defects are predominant[6,11,19,33]:

$$2Al_{Al}^{x} + 6Fe_{Al}^{x} + 12O_{O}^{x} \rightarrow 2Al_i^{\bullet\bullet\bullet} + 6Fe'_{Al} + 9O_{O}^{x} + 3/2O_2(g) \quad (1)$$

or ionized oxygen vacancies if Schottky defects are predominant[6,11,17]

$$2Fe_{Al}^{x} + 3O_{O}^{x} \rightarrow 2Fe'_{Al} + V_o^{\bullet\bullet} + 2O_{O}^{x} + 1/2O_2(g) \quad (2)$$

According to the space charge formalism developed by Kliewer and Koehler,[34] the equilibrium defect concentrations (in terms of the number of defects per molecule Al_2O_3) in the bulk (i.e. at a distance $x \rightarrow \infty$ far from the grain boundary) of alumina are given by:

$$[Al_i^{\bullet\bullet\bullet}]_\infty = \exp\left[\frac{-(g_{Al_i^{\bullet\bullet\bullet}} + 3e\Phi_\infty)}{kT}\right] \quad (3)$$

$$[V_o^{\bullet\bullet}]_\infty = 3\exp\left[\frac{-(g_{V_o^{\bullet\bullet}} + 2e\Phi_\infty)}{kT}\right] \quad (4)$$

The formation free energies $g_{Al_i^{\bullet\bullet\bullet}}$ and $g_{V_o^{\bullet\bullet}}$ are defined relative to the grain boundary sites. The formation energy $g_{V_o^{\bullet\bullet}}$ should not be confused with the energy to remove an oxygen ion from its normal site to infinity as reported in defect energy calculations.[26–28] The electrostatic potential difference between the bulk (Φ_∞) and the grain boundary, where it is referenced to zero ($\Phi_0 = 0$), is the space charge potential Φ_∞. In both situations, the electrostatic potential difference between the bulk and the grain boundary is obtained by applying the bulk electroneutrality conditions:

$$3[Al_i^{\bullet\bullet\bullet}]_\infty = [Fe'_{Al}]_\infty \quad (5)$$

or

$$2[V_o^{\bullet\bullet}]_\infty = [Fe'_{Al}]_\infty \quad (6)$$

The results show that the space charge potential in the bulk is determined by the aliovalent solute content, the formation free energy of the compensating defect and the temperature. It is given, respectively, by:

$$3e\Phi_\infty = -g_{Al_i^{\bullet\bullet\bullet}} - kT\ln\left(\frac{[Fe'_{Al}]_\infty}{3}\right) \quad (7)$$

or by

$$2e\Phi_\infty = -g_{V_o^{\bullet\bullet}} - kT\ln\left(\frac{[Fe'_{Al}]_\infty}{6}\right) \quad (8)$$

for aluminium interstitials or oxygen vacancies as compensating defects. To estimate the space charge potential, we need the separate free formation energies of $g_{Al_i^{\bullet\bullet\bullet}}$ and of $g_{V_o^{\bullet\bullet}}$ for the respective compensating defects relative to the boundary. As we have discussed previously, there are no reliable data or direct calculations for $g_{Al_i^{\bullet\bullet\bullet}}$ and $g_{V_o^{\bullet\bullet}}$. As the sign of the space charge potential is only necessary in our analysis, we have used a method already described in the study of ionic double layers at the surface of Mg-doped alumina,[35] to choose $g_{Al_i^{\bullet\bullet\bullet}}$ and $g_{V_o^{\bullet\bullet}}$. From the theoretical calculations of the Schottky defect energies published by several authors[26–28] we have estimated $g_{V_o^{\bullet\bullet}}$ and $g'''_{V_{Al}}$ taking the ratio $g'''_{V_{Al}}/g_{V_o^{\bullet\bullet}}$ to be equal to the lattice Al^{3+} upon O^{2-} formation energies ratio, and then, from the calculated Al Frenkel defect energies[26–28] we have estimated $g_{Al_i^{\bullet\bullet\bullet}}$. Finally, we have chosen the lowest obtained values, respectively, $g_{Al_i^{\bullet\bullet\bullet}} = 5.81$ eV and $g_{V_o^{\bullet\bullet}} = 3.12$ eV. At 1400 °C, kT has a value of 0.144 eV.

4.2. Defects and solutes redistribution

From equations (7) and (8) two negative values of $e\Phi_\infty$ were obtained ($e\Phi_\infty = -1.6$ eV and $e\Phi_\infty = -2$ eV, respectively, for $Al_i^{\bullet\bullet\bullet}$ or $V_o^{\bullet\bullet}$ as compensating defects) for the level of Fe doping used in the present work. Thus, if the effect of Fe'_{Al} dominates over the intrinsic defects, the space charge potential in the specimen is negative and the grain boundary charge is positive. This situation corresponds to a segregation of acceptor solutes Fe'_{Al} and other minor defects of negative effective charge, such as V'''_{Al} and O''_i, together with a depletion of $Al_i^{\bullet\bullet\bullet}$ and $V_o^{\bullet\bullet}$ in the space charge layers. This is in agreement with the conclusion of Tiku and Kroeger[8] that in Fe-doped Al_2O_3, there is no appreciable grain boundary segregation of Fe'_{Al} and this corresponds, as in the case of Mg-doped alumina,[12–14] to a grain boundary with a positive charge due to an excess of Al^{3+} ions and other defects of positive effective charge, such as $Al_i^{\bullet\bullet\bullet}$. In this case, the $Al_i^{\bullet\bullet\bullet}$ defect concentration in the grain boundary is increased proportionally to the dopant addition, as long as it remains as a solute Fe'_{Al} in the space charge region, so that the grain boundary diffusion kinetics, pertinent to sintering in reducing conditions[10] and to the early stage of creep in air, were enhanced as we observed (Fig. 1 a). Indeed, the initial grain size being smaller for undoped alumina the true strain rate was faster in the very early stage of deformation in comparison to 0.5 at.% Fe-doped alumina. However, the true strain rate remained higher for the Fe-doped alumina in the deformation range $\varepsilon = [-3, -15\%]$.

Here the grain boundary regions have been microanalysed and they have been found to be Fe-dopant enriched regions. This observation is consistent with previous studies on isovalent and aliovalent doping.[4,5] According to our previous discussion, Fe^{2+} ions have segregated as Fe'_{Al} to the space charge region. However, here the ability to distinguish between the strictly grain boundary and the space charge regions was beyond the capability of our microanalysis system. Indeed, under the conditions of observation the spot size was about 5 nm. Nevertheless, the microanalysis information are favourable to the conclusion of the iron been preferentially segregated in the grain boundary regions, whatever its valence. The smaller concentration of the neutral Fe^{x}_{Al} was constant in the bulk (Fig. 2.) and in the space charge region. As for the observed iron spinel precipitates, they resulted from the lack of solubility of Fe^{2+} species, which is very low although not known in the subgrain boundary region. There was no observation of cavity formation at the new interface resulting from the precipitation. Hence, this interface seemed neither to lower, nor to speed up the matter transport. The major observed grain boundary inclusion configurations showed an efficient pinning of the alumina boundaries by spinel, as illustrated in Fig. 3.

4.3. Oxidation of Fe^{2+} and the consequences of oversized species segregation on creep

The change of the creep strain rate in the Fe-doped alumina shall now be discussed in terms of iron oxidation state evolution, defect nature and defect evolution during deformation. Some indications of Fe^{2+} oxidation to Fe^{3+} correspond to the specimen bulk colouration change, in the narrow strain range [−14, −17%], from dark-green to a bright red colour, indicating now an excess of Fe^{3+} cations. During creep in air, vacancy or interstitial populations can decrease, respectively, in the anion or in the cation sublattices by atmospheric interaction. If Schottky or Frenkel defects are, respectively, predominant, oxygen diffused in the grain boundaries and resulted in the oxidation of the Fe^{2+} population following the reactions expressed in quasi-chemical terms:

$$1/2O_2(g) + 2Fe'_{Al} + V_o^{\bullet\bullet} + 2O^x_O \rightarrow 3O^x_O + 2Fe^x_{Al} \quad (9)$$

$$3/2O_2(g) + 9O^x_O + 2Al_i^{\bullet\bullet\bullet} + 6Fe'_{Al} \rightarrow 12O^x_O + 2Al^x_{Al} + 6Fe^x_{Al} \quad (10)$$

This mechanism occurred actively along the pathway of oxygen atomic transport, i.e. in the grain boundary and subgrain boundary vicinity. This oxidation mechanism, acting during creep in air, resulted in a decrease of the Fe^{2+} cation population. A high strain rate was maintained as long as the corresponding Fe'_{Al} population was large enough to sustain a high $Al_i^{\bullet\bullet\bullet}$ defect population in the grain boundary. The onset of the second stage is associated with this population decreasing under a limit corresponding to the situation where the neutral foreign defects were the major species ($[Fe^x_{Al}] \gg [Fe'_{Al}]$) (see Fig. 1). Eventually, the Fe oxidation favoured the Fe^{3+} to migrate into the grain boundary, being present as Fe^x_{Al} species. Tiku and Kroeger[8] have shown that when $[Fe^x_{Al}] \gg [Fe'_{Al}]$, Fe^x_{Al} populations in the bulk and in the space charge region can be very low, compared to the average dopant level, for fine grain size samples, most of the oversized isovalent Fe^{3+} cations having now segregated to the grain boundaries, as a result of elastic effects. Cation size effects are important for the segregation mechanism of the oversized dopant; the Fe^{3+} cation size is about 0.065 nm[10,36] whereas Al^{3+} is 0.054 nm.[10,37] It has been recently suggested that, as for large oversize dopant such as Zr, Y and elements in the lanthanide series,[10,37–39] Fe^{3+} cations segregate to the alumina grain boundaries, and they can retard grain boundary transport by blocking of rapid diffusion pathways.

Opposite to that behaviour was the evolution of undoped alumina under creep in the same conditions. According to Fig. 1, a steady state creep was reached for the undoped alumina in the true strain range [−10, −20%]. Indeed, in this material neither the structure of the grain boundary nor the structure of the space charge subgrain boundary region underwent an evolution in this true strain range. The defect population remained identical. Grain size growth and cavitation were possible but they had, at this stage, a minor role.

5. Conclusion

Iron doping has modified the alumina creep behaviour, in air. Substitutional Fe^{2+} cation segregated in the space charge subgrain boundary region and it improved grain boundary controlled diffusion creep through an increase of $Al_i^{\bullet\bullet\bullet}$ population in a positive grain boundary. Iron valence did control the defect population and distribution and consequently the grain boundary diffusive mass transport accommodating the strain. Under the described conditions, this beneficial effect was limited by the oxidation of Fe^{2+} cation population during creep in air. The described deformation behaviour has to be associated to those iron population changes. Those changes would occur by simple thermal heating but the time scale would be very much longer. Here the strain sped up the overall matter transport. The association of strain and oxidation was responsible of the decrease of strain rate during creep test in air.

References

1. Hou, L. D., Tiku, S. K., Wang, H. A. and Kroeger, F. A., Conductivity and creep in acceptor-dominated polycrystalline Al_2O_3. *J. Mater. Sci.*, 1977, **14**, 1877–1889.
2. Lessing, P. A. and Gordon, R. S., Creep of polycrystalline alumina, pure and doped with transition metal impurities. *J. Mater. Sci.*, 1977, **12**, 2291–3020.
3. Ikuma, Y. and Gordon, R. S., Effect of doping simultaneously with iron and titanium on the diffusional creep of polycrystalline Al_2O_3. *J. Am. Ceram. Soc.*, 1983, **66**(2), 139–142.
4. Tartaj, J. and Messing, G. L., Anisotropic grain-growth in alpha Fe_2O_3-doped alumina. *J. Eur. Ceram. Soc.*, 1997, **17**, 719–725.
5. Bataille, A., Addad, A., Crampon, J. and Duclos, R., Deformation behaviour of iron-doped alumina. *J. Eur. Ceram. Soc.*, 2005, **25**, 857–862.
6. Rao, W. R. and Cutler, I. B., Effect of iron oxide on the sintering kinetics of Al_2O_3. *J. Am. Ceram. Soc.*, 1973, **56**(11), 588–593.
7. Wang, H. A. and Kroeger, F. A., Chemical diffusion in polycrystalline Al_2O_3. *J. Am. Ceram. Soc.*, 1980, **63**(11–12), 613–619.

8. Tiku, S. K. and Kroeger, F. A., Effects of space charge, grain-boundary segregation, and mobility differences between grain-boundary and bulk on the conductivity of polycrystalline Al_2O_3. *J. Am. Ceram. Soc.*, 1980, **63**(3–4), 183–189.
9. Zhao, J. and Harmer, M. P., Sintering of ultra-high purity alumina doped simultaneously with MgO and FeO. *J. Am. Ceram. Soc.*, 1987, **70**(12), 860–866.
10. Drahus, M. D., Chan, H. M., Rickman, J. M. and Harmer, M. P., Densification and grain-growth of Fe-doped and Fe/Y-codoped alumina: Effect of Fe valency. *J. Am. Ceram. Soc.*, 2005, **88**(12), 3369–3375.
11. Jeong, J. W., Han, J. H. and Kim, D. Y., Effect of electric field on the migration of grain-boundaries in alumina. *J. Am. Ceram. Soc.*, 2000, **83**(4), 915–918.
12. Kingery, W. D., Plausible concepts necessary and sufficient for interpretation of ceramic grain-boundary phenomena: I, Grain-boundary characteristics, structure and electrostatic potential. *J. Am. Ceram. Soc.*, 1974, **57**(1), 1–8.
13. Kingery, W. D., Bowen, H. K. and Uhlmann, D. R., *Introduction to Ceramics* (*2nd ed.*). John Wiley and Sons, 1976, pp. 190–197.
14. Mac Colm, I. J. and Clark, N. J., *Forming, Shaping and Working of High Performance Ceramics*. Chapman and Hall, 1986, pp. 29, 54.
15. Yang, D. and Conrad, H., Plastic deformation of fine-grained Al_20_3 in the presence of an electric field. *Scripta Mater.*, 1999, **41**(4), 397–401.
16. Conrad, H., Space charge and the dependence of the flow stress of ceramics on an applied electric field. *Scripta Mater.*, 2001, **44**, 311–316.
17. Choi, J. I., Han, J. H. and Kim, D. Y., Effect of titania and lithia doping on the boundary migration of alumina under an electric field. *J. Am. Ceram. Soc.*, 2003, **86**(4), 640–643.
18. Carry, C. and Mocellin, A., Structural superplasticity in single phase crystalline ceramics. *Ceram. Int.*, 1987, **13**, 89–98.
19. Gordon, R. S., Understanding defect structure and mass transport in polycrystalline Al_2O_3 and MgO via the study of diffusional creep. In *Advances in Ceramics*, *Vol. 10*, ed. W. D. Kingery. American Ceramic Society, Columbus, OH, 1984, pp. 418–437.
20. Kroeger, F. A. and Vink, H. J., *Solid State Physics*, *Vol. 3*, ed. F. Seitz and D. Turnbull. Academic Press, New York, 1956, pp. 307–435.
21. Harding, J. H., Atkinson, K. J. W. and Grimes, R. W., Experiment and theory of diffusion in alumina. *J. Am. Ceram. Soc.*, 2003, **86**(4), 554–559.
22. Atkinson, K. J. W., Grimes, R. W., Levy, M. R., Coull, Z. L. and English, T., Accommodation of impurities in α-Al_2O_3 and α-Cr_2O_3 and α-Fe_2O_3. *J. Eur. Ceram. Soc.*, 2003, **23**, 3059–3070.
23. Matsunaga, K., Tanaka, T., Yamamoto, T. and Ikuhara, Y., First-principles calculations of intrinsic defects in Al_2O_3. *Phys. Rev. B*, 2003, **68**, 085110.
24. Matsunaga, K., Nakamura, A., Yamamoto, T. and Ikuhara, Y., First-principles study of defect energetics in titanium-doped Alumina. *Phys. Rev. B*, 2003, **68**, 214102.
25. Matsunaga, K., Nakamura, A., Yamamoto, T. and Ikuhara, Y., Theoretical study of defect structure in pure and titanium-doped alumina. *Solid State Ionics*, 2004, **172**, 155–158.
26. Dienes, G. J., Welch, D. O., Fischer, C. R., Hatcher, R. D., Lazareth, O. and Samberg, M., Shell-model calculation of some point defect properties in α-alumina. *Phys. Rev. B*, 1975, **11**, 3060–3066.
27. Catlow, C. R., James, R., Mackrodt, W. C. and Stewart, R. F., Defect energetics in α-Al_2O_3 and rutile TiO_2. *Phys. Rev. B*, 1982, **25**(2), 1006–1026.
28. Mackrodt, W. C., Calculated point defect formation, association and migration energies in MgO and α-Al_2O_3. In *Advances in Ceramics*, *Vol. 10*, ed. W. D. Kingery. American Ceramic Society, Columbus, OH, 1984, pp. 62–78.
29. Jacobs, P. W. M. and Kotomin, E. A., Defect energies in pure corundum and for corundum doped with transition metal ions. *Philos. Mag. A*, 1993, **68**, 695–709.
30. Jacobs, P. W. M. and Kotomin, E. A., Modeling of point defect in corundum crystals. *J. Am. Ceram. Soc.*, 1994, **77**(10), 2505–2508.
31. Grimes, R. W., Solution of MgO, CaO, and TiO2 in α-Al2O3. *J. Am. Ceram. Soc.*, 1994, **77**(2), 378–385.
32. Lagerlöf, K. D. P. and Grimes, R. W., The defect chemistry of sapphire (α-Al2O3). *Acta Mater.*, 1998, **46**(16), 5689–5700.
33. Dutt, B. V. and Kroeger, F. A., High temperature defect structure in iron-doped α-alumina. *J. Am. Ceram. Soc.*, 1975, **58**(12), 474–476.
34. Kliewer, K. L. and Koehler, J. S., Space charge in ionic crystals. I. General approach with application to NaCl. *Phys. Rev. A*, 1965, **140**(4), 1226–1240.
35. Mukhopadhyay, S. M. and Blakely, J. M., Ionic double layers at the surface of magnesium-doped aluminium oxide: Effect on segregation properties. *J. Am. Ceram. Soc.*, 1991, **74**(1), 25–30.
36. Thompson, A. M., Soni, K. K., Chan, H. M., Harmer, M. P., Williams, D. B., Chabala, J. M. and Levi-Setti, R., Dopant distributions in rare-earth-doped alumina. *J. Am. Ceram. Soc.*, 1997, **80**(2), 373–376.
37. Wakai, F., Nagano, T. and Iga, T., Hardening in creep of alumina by zirconium segregation at the grain-boundary. *J. Am. Ceram. Soc.*, 1997, **80**(9), 2361–2366.
38. Bruley, J., Cho, J., Chan, H. M., Harmer, M. P. and Rickman, J. M., Scanning transmission electron microscope analysis of grain-boundaries in creep resistant yttrium and lanthanum-doped alumina microstructures. *J. Am. Ceram. Soc.*, 1999, **82**(10), 2865–2870.
39. Lin, Y. Z., Wang, C., Chan, H. M., Rickman, J. M. and Harmer, M. P., Codoping of alumina to enhance creep resistance. *J. Am. Ceram. Soc.*, 1999, **82**(6), 1497–1504.